JOURNAL OF COMPUTATIONAL PHYSICS 41, 89–114 (1981)

Three-Dimensional Ship Wave Generation Using an Efficient Finite Difference Scheme with Double Model Linearization

SAMUEL OHRING

David W. Taylor Naval Ship Research and Development Center, Bethesda, Maryland 20084

Received June 27, 1980

An efficient three-dimensional implicit finite difference scheme with a double model velocity linearization of the free surface conditions is used to model three-dimensional potential flow about an abruptly started surface piercing ship moving at constant speed in a channel of initially calm water. The numerical scheme is efficient with respect to both computer storage and time mainly due to the use of the direct matrix imbedding method. The double model velocity linearization should yield more accurate results, except perhaps for very high Froude numbers, than the standard free stream velocity linearization. With slight modification, the numerical scheme can compute flow about an accelerating ship. Computed results such as ship wave profiles and wave resistence for four different ship speeds are in generally good agreement with model test experiments. Contour and perspective plots of the generated ship waves are displayed.

1. INTRODUCTION

The problem of wave making and wave resistance of ships has been and is one of the central areas of marine research, e.g. [1–3]. The wave resistence of an accelerating surface piercing ship has been of particular interest in connection with towing-tank experiments. This paper presents a numerical technique for obtaining the transient solution for the potential flow about a ship translating with uniform speed from an abrupt start in calm water in a channel. This problem can be viewed mathematically as an initial boundary-value problem. The abrupt start is viewed as modeling a very rapid acceleration from rest. The numerical technique can handle accelerations and decelerations of the ship, although this is not considered in this paper.

The initial boundary value problem consists of two major parts: (a) the field equation subject to the ship boundary condition, and (b) the free surface equations. In this paper, part (a) is handled numerically by the direct matrix imbedding technique as described in detail in [4]. For part (b) a double model velocity linearization is used. The free surface is linearized in terms of a velocity field in the mean free surface level about the ship obtained from a separate boundary value problem for the potential flow in the channel past the ship and its mirror image (double model)

0021-9991/81/050089-26$02.00/0

Copyright © 1981 by Academic Press, Inc.
All rights of reproduction in any form reserved.

reflected in the mean level. (There is no free surface in this separate problem.) This linearization results in more accurate results than those obtained using a standard free stream velocity linearization as in [5]. Dawson [1] has obtained excellent steady-state results using such a linearization with source panels.

The numerical technique for each time step couples the fast solution of part (a) by the imbedding technique to the solution of part (b) by Gauss–Seidel point iteration. The coupling ordinarily involves a few iterations in a "predictor–corrector" manner with a convergence test on the vertical fluid velocity at the free surface.

The imbedding technique, which is used to satisfy the ship boundary condition, imbeds the ship in a grid. A Cartesian grid is used to allow very fast, efficient direct solutions to matrix systems involved in the imbedding technique. Since the ship generally will not lie on grid points, special finite differencing must be used in the neighborhood of the ship. This neighborhood includes grid points both on and below the undisturbed mean free surface level (on which the linearized free surface equations are to be satisfied).

Section 2 of this paper describes the mathematical formulation for the initial boundary value problem. Section 3 describes the numerical method. Computed results are presented in Section 4, and Section 5 summarizes conclusions.

2. Mathematical Formulation

Consider a right-handed Cartesian coordinate reference frame fixed to a ship hull translating with uniform speed U in a channel (Fig. 1). (The dimensionless speed of 1 is shown. Distances have been nondimensionalized with respect to the ship length L, and the vector $\mathbf{n} = (n_x, n_y, n_z)$ is the unit outward normal to the hull.) In the discussion that follows the fluid is assumed to be incompressible and the flow to be irrotational, i.e., potential flow.

The problem of obtaining the double model velocity is considered first. This is equivalent to considering potential flow past the ship and its image reflected about the plane $y = 0$. The computational region and ship are thus symmetric about $y = 0$. Since we shall consider a ship symmetric about the plane $z = 0$ in this paper, Fig. 1

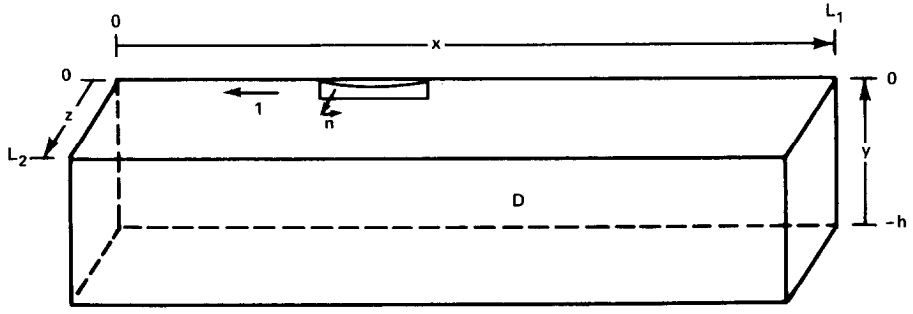

FIG. 1. The computational region.

actually shows one-fourth of the region in which potential flow past the double model (the ship and its reflected image) is to be computed. Of particular interest, for the free-surface linearization, is the potential flow velocity at $y = 0$. As the dimensionless velocity potential Φ $(=x+\hat{\phi})$ and the dimensionless velocity vector (Φ_x, Φ_y, Φ_z) given by $(1+\hat{\phi}_x, \hat{\phi}_y, \hat{\phi}_z)$ have been nondimensionalized in terms of LU and U, respectively, the problem then is to numerically compute the double model velocity vector $(1+\hat{\phi}_x, 0, \hat{\phi}_z)$ in the plane $y = 0$ subject to the following boundary value problem for the region shown in Fig. 1:

$$\hat{\phi}_{xx} + \hat{\phi}_{yy} + \hat{\phi}_{zz} = 0 \qquad \text{in the computational region } D \text{ exterior to the ship,} \tag{1}$$

$$\hat{\phi}_y = 0 \qquad \text{at } y = 0, \tag{2}$$

$$\hat{\phi}_n = -n_x \qquad \text{at the ship hull,} \tag{3}$$

$$\hat{\phi} = 0 \qquad \text{at } y = -h, \tag{4}$$

$$\hat{\phi}_x = 0 \qquad \text{at } x = 0, L_1, \tag{5}$$

$$\hat{\phi}_z = 0 \qquad \text{at } z = 0, L_2, \tag{6}$$

This is a steady state problem with $\hat{\phi}$ time-independent. The subscript n indicates a normal derivative, and $z = L_2$ is the channel sidewall. Equation (2) represents the reflection condition at $y = 0$. Equation (6) at $z = 0$ represents the symmetry condition, and at $z = L_2$, the channel sidewall condition. Equations (4) and (5) are applied far enough away from the ship to be approximately valid. The direct matrix imbedding technique as described in [4] is used to solve numerically this boundary value problem for the velocity vector with components $(1+\hat{\phi}_x, 0, \hat{\phi}_z)$ at $y = 0$. These components are then used in the free surface problem definition which shall now be discussed.

The abrupt start of a surface piercing ship moving at uniform speed and generating ship waves in a channel with fluid initially at rest is modeled with an initial boundary value problem in the following way: First the following dimensionless velocity potential is introduced in terms of $\hat{\phi}$:

$$\tilde{\Phi} = \Phi + \bar{\phi} = x + \hat{\phi} + \bar{\phi} = x + \phi. \tag{7}$$

The free surface conditions for gravity waves are given nondimensionally (see [6]) as

$$\tilde{\Phi}_x \eta_x - \tilde{\Phi}_y + \tilde{\Phi}_z \eta_z + \eta_t = 0 \qquad \text{at} \quad y = \eta, \tag{8}$$

$$\eta/\mathrm{Fr}^2 + \tilde{\Phi}_t + \tfrac{1}{2}(\tilde{\Phi}_x^2 + \tilde{\Phi}_y^2 + \tilde{\Phi}_z^2) + p = c(t) \qquad \text{at} \quad y = \eta. \tag{9}$$

The quantities η, t, and p are the nondimensional free surface elevation, time, and pressure, respectively, and have been scaled by L, L/U, and ρU^2, respectively, ρ being the constant density. The nondimensional Froude number $\mathrm{Fr} = U/\sqrt{gL}$ with g the acceleration due to gravity and c is a time-dependent constant. Setting p to dimensionless atmospheric pressure and assuming no disturbance at infinity makes it

possible to remove the constant $c = \frac{1}{2} + p$ from both sides of Eq. (9). Substituting Eq. (7) for $\tilde{\Phi}$ into Eqs. (8) and (9), and eliminating all quadratic terms involving spacial derivatives of $\hat{\phi}$ and η (i.e., $\hat{\phi}_x \eta_x$, etc.), produces the following free surface equations, now applied at $y = 0$ (exterior to the ship) in Fig. 1 and linearized in terms of the known double model velocities $1 + \hat{\phi}_x$ and $\hat{\phi}_z$ at $y = 0$:

$$\eta_t = -[(1 + \hat{\phi}_x)\eta_x - \phi_y + \hat{\phi}_z \eta_z] \qquad \text{at} \quad y = 0, \tag{10}$$

$$\phi_t = -[\eta/\mathrm{Fr}^2 - \tfrac{1}{2}(\hat{\phi}_x^2 + \hat{\phi}_z^2) + (1 + \hat{\phi}_x)\phi_x + \hat{\phi}_z \phi_z] \qquad \text{at} \quad y = 0. \tag{11}$$

(All velocities have been scaled with respect to U and all coordinate distances with respect to L.)

The following boundary and initial value conditions complete the definition of the initial boundary value problem for the region displayed in Fig. 1:

$$\phi_{xx} + \phi_{yy} + \phi_{zz} = 0 \qquad \text{in the computational region } D \text{ exterior to the ship,} \tag{12}$$

$$\phi_n = -n_x \qquad \text{at the ship hull,} \tag{13}$$

$$\phi_y = 0 \qquad \text{at } y = -h, \tag{14}$$

$$\phi_x = 0 \qquad \text{at } x = 0, L_1, \tag{15}$$

$$\phi_z = 0 \qquad \text{at } z = 0, L_2, \tag{16}$$

$$\eta = 0; \phi = 0 \qquad \text{at } t = 0, \text{ at } y = 0. \tag{17}$$

Equation (14) represents a wall or bed condition at the bottom of the channel. It is stressed that $z = 0$ is a plane of symmetry for the symmetric ship, and therefore for the flow, and that $z = L_2$ is the channel sidewall. Equation (15) is valid as long as waves propagating downstream have not reached the downstream boundary ($x = L_1$). Equation (17) simulates the abrupt start. Equations (10) through (17) represent the initial boundary value problem.

An expression, useful in the numerical computation, can be obtained for the normal derivative of the free surface elevation η at the ship at the undisturbed level $y = 0$. Applying the ship hull condition (Eq. (13)) and taking the normal derivative of Eq. (11) at the ship at $y = 0$ gives

$$\eta_n = -\mathrm{Fr}^2[-\tfrac{1}{2}(\hat{\phi}_x^2 + \hat{\phi}_z^2)_n + \{(1 + \hat{\phi}_x)\phi_x + \hat{\phi}_z \phi_z\}_n]. \tag{18}$$

But

$$(\Phi_l \phi_l)_n = \Phi_l (\phi_l)_n = \{(1 + \hat{\phi}_x)\phi_x + \hat{\phi}_z \phi_z\}_n. \tag{19}$$

Here Φ_l is the arclength derivative of the double model potential Φ ($= x + \hat{\phi}$) along the ship at $y = 0$. ($(\Phi_n)_l$ is zero.) Substituting Equation (19) into Eq. (18) ($\hat{\phi}_{nz} = 0$ at the ship) yields the following expression for η_n in terms of known quantities from the double model computation and a known ϕ_{nl} from Eq. (13):

$$\eta_n = -\mathrm{Fr}^2[-\hat{\phi}_x \hat{\phi}_{nx} + \Phi_l \phi_{nl}] \qquad \text{at the ship at } y = 0. \tag{20}$$

Normal differentiation in the plane $y = 0$ is valid since the ship considered in this paper has its unit outward normal vector at $y = 0$ lying in the plane $y = 0$. This is true (or approximately true) of most ships.

The pressure p below the free surface is given by Bernoulli's law:

$$p = -[\phi_t + \tfrac{1}{2}(2\phi_x + \phi_x^2 + \phi_y^2 + \phi_z^2) + y/\mathrm{Fr}^2]. \tag{21}$$

(The dimensional pressure has been scaled by ρU^2.) The nondimensional wave resistance to the ship's movement through the water is given by

$$C_R = -2 \int_{\text{hull}} p n_x \, dS. \tag{22}$$

The dimensional wave resistance has been scaled by $\rho U^2 A$, where A is the projection of the ship hull surface S (one side) onto the center plane $z = 0$.

3. The Numerical Method

The direct matrix imbedding technique as presented in detail in [4] is used to numerically solve (i) the double model velocity problem (defined by Eqs. (1) through (6)), and (ii) that component of the ship wave problem which is coupled to the solution of the free surface equations in a predictor corrector manner for each time step. This component is defined by Eqs. (12) through (16) with a Dirichlet condition for ϕ at $y = 0$. Both boundary value problems are solved on a three-dimensional Cartesian grid covering the region shown in Fig. 1. (The ship hull surface is not necessarily coincident with grid points.) For the double model problem, the velocity potential $\hat{\phi}$ is obtained numerically at grid points in the plane $y = 0$ from which the double model velocity components $(1 + \hat{\phi}_x, 0, \hat{\phi}_z)$ are calculated at grid points, using second order differencing at $y = 0$. These velocity components are then used for the ship wave problem. For the ship wave problem component, ϕ_y at $y = 0$ is calculated numerically from second order one-sided differencing involving values of ϕ computed in two planes of constant y below $y = 0$ in addition to those values at $y = 0$.

The second order finite difference representation of both boundary value problems gives rise to a large number of simulateneous linear equations whose matrix structure is regular and sparse, except for a relatively small number of perturbed linear equations representing the ship hull boundary condition. The imbedding technique is designed to solve efficiently this slightly perturbed system and, as used here, is based on Woodbury's formula [7]. The technique involves obtaining two very fast direct solutions of a regular sparse system over a small part (near the ship and the free surface) of the Cartesian grid for the region of Fig. 1, plus a solution to a full square matrix system of linear equations of relatively small order. The full matrix C (called the "capacitance" matrix in the literature [7, 8]) must be preprocessed and is of order equal to the number of "irregular stars" or finite difference operators surrounding the

ship hull that are perturbed from the standard second order, seven-point operators. These irregular stars can be formulated in many different ways but those used in [4] incorporated curvature of the ship hull along with the ship hull condition and Laplace's equation. These irregular stars yield second order accuracy.

The three-dimensional grid used is defined as follows: L_1, L_2, and h in Fig. 1 are 6.4, 0.8, and 32/25, respectively (i.e., the region was 6.4 ship lengths long, etc.). A grid with 128 intervals in x, 256 intervals in y, and 16 intervals in z overlays the box region of Fig. 1. Spacing in z expands from the ship to the sidewall of the channel; spacing in the x- and y-directions is uniform with $\Delta x = 0.05$ and $\Delta y = 0.005$. The z-coordinate discretization consists of eight mesh intervals with spacing $\Delta z = 0.025$ from $z = 0$ to $z = 0.2$, four mesh intervals with spacing $\Delta z = 0.05$ from $z = 0.2$ to $z = 0.4$, and four mesh intervals with spacing $\Delta z = 0.1$ from $z = 0.4$ to $z = 0.8$. For increased efficiency in the imbedding technique [4] uniform spacing in the x-direction was chosen to permit use of the Fast Fourier Transform, and uniform spacing in the y-direction made possible the calculation of the solution only where it was required (near the ship hull and the free surface). The uniform spacings in the x- and y-directions contribute to a much faster solution process. The nature of the stretched spacing in z, in which the size of adjacent intervals is either doubled, kept the same, or halved, allows one to retain the use of a quite efficient imbedding technique.

The ship hull used in this paper is known as the Wigley 1805A [9] and is represented by the analytic function

$$z = H(x, y) = \pm(3/64)(1 - 256y^2)(1 - 6.4(x - x_c)^2 + 9.6(x - x_c)^4). \tag{23}$$

When a ship hull is described by an analytic or piecewise anlytic function, local curvature of the ship hull can be incorporated into the irregular stars as was done here. Techniques exist for representing hulls given by discrete points as piecewise analytic functions [10]. The normal vector to the ship hull described by Eq. (23) does not exist at the intersection of the hull with the plane $z = 0$. Therefore this intersection is taken to lie halfway between grid points in x. The hull is taken to be twenty grid intervals in length along x and twelve and one-half intervals in depth y. The half-beam equal to 3/64 is just under two grid intervals wide in the z-direction, with x_c (the center of the ship) taken to be 2.025. For the double model problem 260 irregular stars were alongside the ship, including 20 in the plane $y = 0$. Additionally 46 irregular stars (centered in the plane $z = 0$) surrounded the ship's intersection with $z = 0$ for a total of 306 irregular stars. In the ship wave problem the total number of irregular stars used by the imbedding technique is 284 (rather than 306) because of the Dirichlet condition for ϕ at $y = 0$. This necessitates additional computer preprocessing for an additional capacitance matrix C_S for the ship wave problem. Figure 2 shows the computer-drawn grid and hull contour in the mean level plane $y = 0$.

An implicit second order time difference scheme known as Euler's modified method is used to advance the free surface Eqs. (10) and (11) at each time step for the ship wave problem. An explicit scheme is not chosen since it ordinarily requires

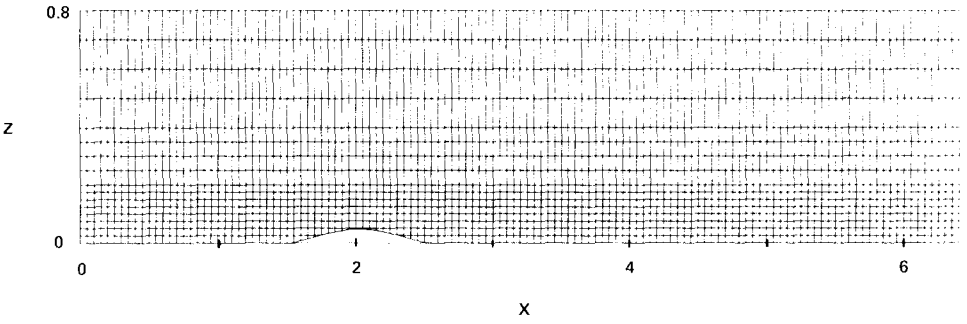

FIG 2. The grid and hull contour in the plane $y = 0$.

very small time steps for stability. If the right sides of Eqs. (10) and (11) are denoted by F and G, respectively, then the scheme is

$$ {}^{(i)}\eta^{n+1} = \eta^n + (\Delta t/2)[{}^{(i)}F^{n+1} + F^n] + O((\Delta t)^2, (\Delta x)^2, (\Delta z)^2) \qquad \text{at} \quad y = 0, \tag{24} $$

$$ {}^{(i)}\phi^{n+1} = \phi^n + (\Delta t/2)[{}^{(i)}G^{n+1} + G^n] + O((\Delta t)^2, (\Delta x)^2, (\Delta z)^2) \qquad \text{at} \quad y = 0, \tag{25} $$

where Δt is the time step, F and G are evaluated at time levels n and $n+1$ (with $t^{n+1} = t^n + \Delta t$), and the left-hand superscript (i) is the iteration counter for new values at time t^{n+1}. Second order spatial differencing, ordinarily central, is used for F and G. Equations (24) and (25) are applied at all grid points of $y = 0$.

The typical calculation for a new time level $n+1$ (based on known values at time level n) is described as follows: Eq. (24) is solved by Gauss–Seidel point iteration for ${}^{(i)}\eta^{n+1}$ for all grid points at $y = 0$. These values of ${}^{(i)}\eta^{n+1}$ are then substituted into Eq. (25) which is then solved by Gauss–Seidel point iteration for ${}^{(i)}\phi^{n+1}$ at all grid points of $y = 0$. These values of ${}^{(i)}\phi^{n+1}$ at $y = 0$ serve as a Dirichlet condition for the boundary value problem, defined by Eqs. (12) through (16), which is solved for ${}^{(i)}\phi_y^{n+1}$ at $y = 0$ by the imbedding technique. This completes the (i)th computational cycle and is followed by a convergence test for the new time level $n+1$. If the test is not satisfied, these values ${}^{(i)}\phi_y^{n+1}$ at $y = 0$ are substituted into Eq. (24) and the $(i+1)$st computational cycle starts. The convergence test for the new time level $n+1$ is satisfied when

$$ |{}^{(i)}\phi_y^{n+1} - {}^{(i-1)}\phi_y^{n+1}|/|{}^{(i)}\phi_y^{n+1}| < \varepsilon_1 \qquad \text{or} \qquad |{}^{(i)}\phi_y^{n+1}| < \varepsilon_2 \tag{26} $$

for all grid points at $y = 0$. (Values at time level n are used for $(i) = (0)$ values.) The same type of convergence conditions, with different values of ε_1 and ε_2, are used to determine convergence of the Gauss–Seidel point iteration for η and ϕ within each computational cycle. When all convergence conditions are satisfied, the latest iterates for ϕ_y, η, and ϕ become the actual values at time level $n+1$. Convergence for a new time level $n+1$ typically requires three or four computational cycles.

The time step used throughout (unless otherwise specified) was Δt equal 0.03. In inequality (26), ε_1 and ε_2 were 0.05 and 0.001, respectively. For the Gauss–Seidel

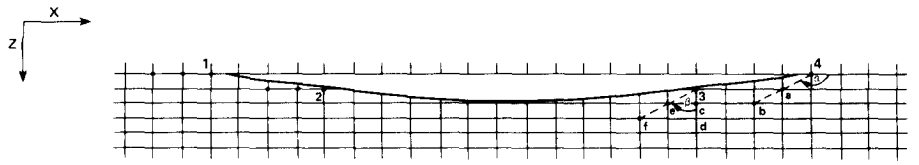

FIG. 3. The local grid about the hull at $y = 0$.

point iterations for η and ϕ, ε_1 and ε_2 were 0.001 and 0.0005, respectively. Typically the maximum number of Gauss–Seidel iterations (always in the first cycle) for either ${}^{(i)}\eta^{n+1}$ or ${}^{(i)}\phi^{n+1}$ is about six. This number usually decreases rapidly in the following two or three cycles within a time step.

The use of a Cartesian grid (required for the efficiency of the imbedding technique) requires very special care in the finite differencing for Eqs. (24) and (25) in the immediate vicinity of the surface piercing ship. Central differencing for x- and z-derivatives is used where possible. Since terms with x-derivatives (i.e., $(1+\hat{\phi}_x)\eta_x$, $(1+\hat{\phi}_x)\phi_x$) dominate those with z-derivatives (i.e., $\hat{\phi}_z\eta_z, \hat{\phi}_z\phi_z$) in Eqs. (10) and (11), finite differencing in x at grid points 1–4 in Fig. 3 is of particular concern. At points 1 and 4, differencing in x must avoid use of Eq. (13), since the normal vector to the hull's surface is not defined at the sharp edges. At point 1 one-sided second order upstream differencing in x is employed. Upstream differencing for x-derivatives must also be used at points 3 and 4, since waves propagate downstream. At point 4 x-derivatives for a quantity Q (such as η or ϕ) were computed according to

$$(Q_x)_4 = (Q_A)_4/\cos\alpha, \tag{27}$$

where A represents the direction increasing along the dashed line from point 4 to points a and b in Fig. 3. Numerically $(Q_A)_4$ is a one-sided second order upstream difference of Q using values at 4, a and b (equally spaced in the A direction). (Symmetry makes the z-derivatives at points 1 and 4 equal zero.)

Grid points 2 and 3 present particular problems which can be handled in a number of ways. In this paper at point 3

$$(Q_x)_3 = (Q_A)_3/\cos\alpha + (Q_z)_3\cot\beta \tag{28}$$

using values of Q at 3, e, f, c, d. At point 2 a one-sided second order upstream difference in x was used.

FIG. 4. The z-derivatives alongside the hull.

The z-derivatives at grid points adjacent to the hull are discretized in the following way (see Fig. 4) using Eqs. (20) and (13): Along the dashed line(s) normal to the body at P in Fig. 4, a one-sided second order finite difference is taken at the body point P, using values at P and the points marked with asterisks. (The values at the asterisks are obtained from second order Lagrangian interpolation in the x-coordinate direction using values at i, j, k and l, m, n.) From this finite difference formula for $(Q_n)_P$ an expression for Q at point P is obtained which, along with values of Q at point j and m, is used in a second order difference centered at point j for $(Q_z)_j$. This discretization has worked nicely.

It is possible and perhaps desirable for the x-derivative discretization discussed for points 2 and 3 to use the hull normal conditions of Eqs. (20) and (13). Further experimentation with finite difference operators is certainly possible. For submerged non-surface piercing bodies generating surface waves, these special discretizations for the free surface equations are obviously not required.

Numerical computations for p and C_R in Eqs. (21) and (22), respectively, are second order accurate. Quantities such as ϕ, ϕ_x, etc. at the ship hull are obtained in terms of computed grid values with an editing process described in [4].

4. Results

Results were obtained for the four Froude numbers $\mathrm{Fr} = 0.503, 0.45, 0.385, 0.32$ for the Wigley 1805A hull (renamed Model 2891 in [9]) given by Eq. (23). Dimensionally this hull has a length L equal to 16 ft, a beam B of 1.5 ft, and a 1.0 ft draft D. Its block coefficient is 0.392 (its volume equals $0.392\,LBD$).

Numerical results will be compared with observed data and values from steady state, analytic, "thin ship" theory [11, pp. 38–47; 9]. In thin ship theory the ship is assumed so thin that the hull condition (Eq. (13)) is applied at $z = 0$, and the free surface Eqs. (8) and (9) are linearized in terms of the free stream velocity U with no waves upstream of the ship permitted. The numerical values obtained should be closer to observed values than are the thin ship values.

The influence of the sidewalls and the bed of the channel (Fig. 1, which shows half the channel) on the local flow solution about the ship was considered negligible, since (a) the depth h (equal to 32/25) of the channel is much greater than half the maximum ship wave length (see [6]) for the cases considered, and (b) the sidewalls are 0.8 of a ship length from the center plane $z = 0$ which is more than 16 times larger than the half-beam of the ship thus allowing waves to reflect downstream off the sidewalls.

Figure 5 shows numerically computed wave profiles alongside and at the hull compared with steady state, observed and thin ship theory profiles at the hull [9] for the four Froude numbers considered. (This and all the following figures have been computer drawn using the Calcomp 936 plotter.) Here "alongside" means the numerically computed elevation η at the nearest grid points alongside the hull (i.e., the points i, j, k, etc. in Fig. 4, and points 2 and 3 in Fig. 3), whereas "at the hull"

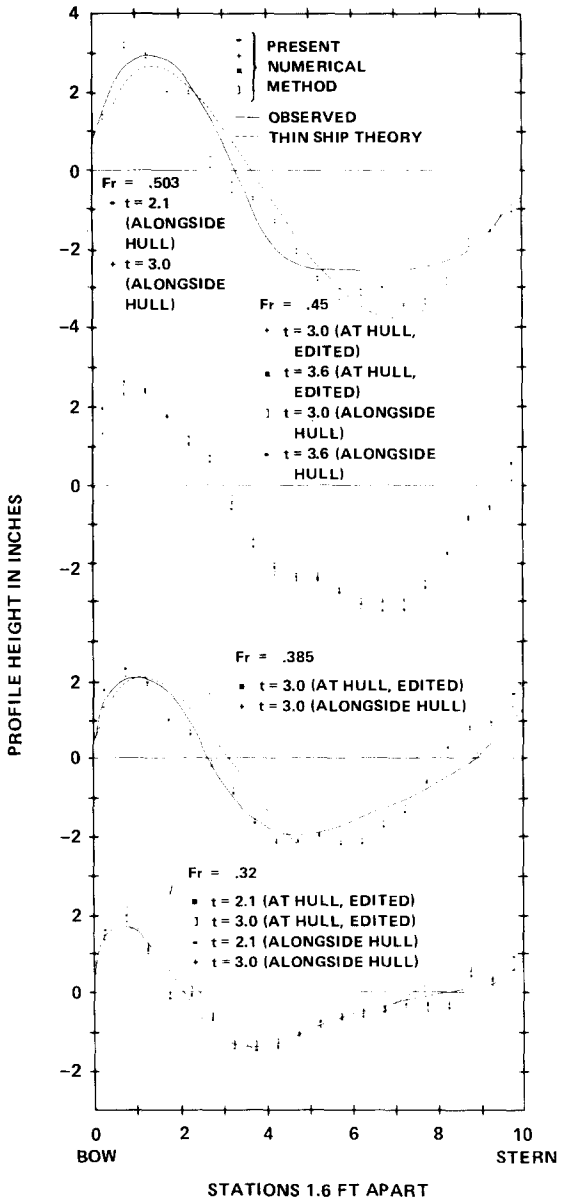

FIG. 5. Wave profiles alongside and at the hull for the four Froude numbers.

means edited values of η at points P at the hull (in Fig. 4). This distinction is necessary since the hull does not ordinarily lie on grid points. Values of η at points P are obtained from numerical values of η at grid points in the field, using the normal derivative condition of Eq. (20) in the manner of the discussion for Fig. 4. For the relatively late times t indicated, the numerical wave profiles generally agree with the

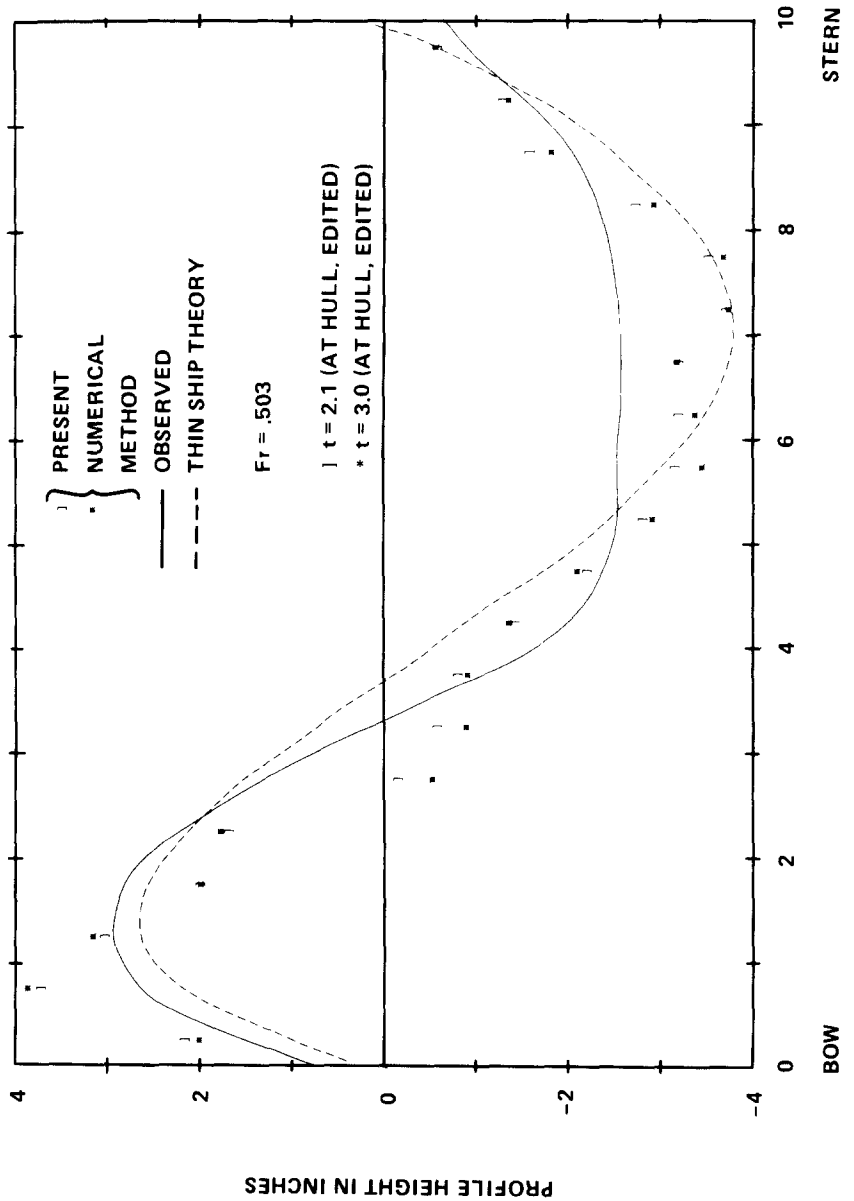

FIG. 6. Wave profiles at the hull for Fr = 0.503.

steady-state observed profiles better than do the steady-state thin ship profiles for all four cases. Also there is very little difference between the numerical wave profiles alongside and at the hull except for $Fr = 0.503$, as seen by comparing Fig. 5 for $Fr = 0.503$ with Fig. 6. The numerical bow wave is not as accurate for $Fr = 0.503$ when compared to the other Froude numbers. However, the numerical stern wave is excellent for $Fr = 0.503$. The fourth numerical data points from the bow and stern ends correspond to grid points 2 and 3, respectively, in Fig. 3. Except for the fourth bow data point (corresponding to grid point 2) for $Fr = 0.32$ and 0.503, the special discretizations used at grid points 2 and 3 seem to have worked reasonably well. It is felt that incorporating Eq. (20) into the discretization for the x-derivative at grid point 2 should improve its accuracy. Steady-state observed and thin ship theory data were not available for $Fr = 0.45$. The time t corresponds directly to the distance the ship has moved after its abrupt start at t equal zero (e.g., $t = 2$ indicates the ship has moved two ship lengths).

Figure 7 shows the numerically computed wave resistance C_R plotted versus time t and compared with the steady state, observed values [9] for the four cases. The observed, steady state values are 0.0044341, 0.0040256, 0.0023619, and 0.0008414 for Fr equal to 0.503, 0.45, 0.385, and 0.32, respectively. The steady state, thin ship theory values (not drawn) are 0.004875, 0.0048076, 0.002740, and 0.0004193 for Fr equal to 0.503, 0.45, 0.385, and 0.32, respectively. After the initial transient effects, the wave resistance curves for the higher Froude numbers (higher speed cases) $Fr = 0.503$ and 0.45 are approximately steady-state beyond $t = 2.0$ and are quite close to the observed, steady state values. Numerical values for C_R at the last time steps computed are 0.00415 and 0.00370 for Fr equal to 0.503 (at $t = 3.0$) and Fr equal to 0.45 (at $t = 3.6$), respectively, and represent a considerable improvement over the steady-state thin ship theory values for these Froude numbers.

The wave resistance curves for the smaller Froude numbers $Fr = 0.385$ and 0.32 show high frequency fluctuations about mean curves having a longer period oscillation. (The words "oscillation" and "fluctuation," as used in the following discussion, are not interchangeable as they have their own separate meanings just defined.) For the thin ship theory approximations, Wehausen [12] has obtained an asymptotic expansion for large time for the wave resistence of a thin ship abruptly started from rest. This asymptotic expansion predicts that, after initial transient effects, the wave resistance curves will be oscillatory in time about steady state values with oscillations of constant wave length for each Froude number with the wave length increasing with increasing Froude number. Additionally, this expansion predicts that the amplitude of the oscillations decreases with increasing Froude number and with increasing time. This asymptotic expansion up to terms of $O(1/t^2)$ gives the following dimensionless wave length of the oscillations

$$\lambda = 8\pi \, \mathrm{Fr}^2. \tag{29}$$

It seems reasonable that this asymptotic expansion might give insight into the behavior of the wave resistance for the problem we are considering: that of a double

model velocity linearization for the free surface with an exact body condition for the ship hull. Some similarities to the asymptotic expansion can be seen in the mean resistance curves (after averaging out the high-frequency fluctuations) for $Fr = 0.32$ and 0.385, with $Fr = 0.32$ showing approximately one-half of an oscillation. (The calculation for $Fr = 0.385$ does not go far enough to approximately determine the wave length of the oscillation.) $Fr = 0.32$ appears to be in good agreement with Eq. (29). The mean wave resistance curve for $Fr = 0.385$ exhibits an oscillation of

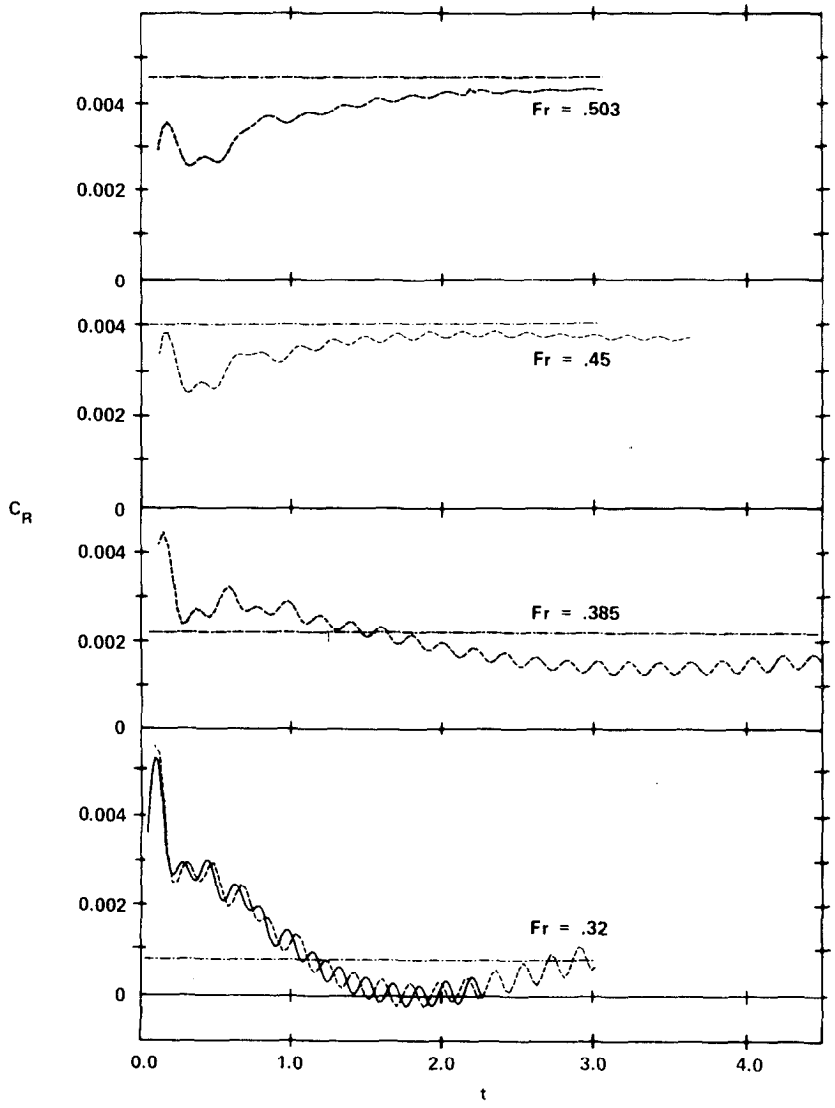

FIG. 7. Wave resistance C_R versus time t for the four Froude numbers. (– – –, numerical C_R; ——, numerical C_R using $\Delta t = 0.015$; — · — · , observed, steady-state C_R).

longer wave length and smaller amplitude than that for $Fr = 0.32$ which is qualitatively in agreement with Welhausen's expansion. The expansion predicts negligible oscillations for higher Froude numbers such as $Fr = 0.45$ and 0.503, which is also the case for the numerical wave resistance curves for these Froude numbers in Fig. 7. To run $Fr = 0.32$ and 0.385 to steady state would be prohibitively expensive. Wave resistance oscillations are due to a periodic rise and fall of the stern wave at the hull. After initial transient effects, the wave profiles for all the Froude number cases considered become approximately steady-state quite quickly, except at the stern for the smaller Froude numbers. When the stern wave is higher, the wave resistance is smaller because the greater fluid pressure at the stern pushes the hull in its direction of movement. When the stern wave is lower, the wave resistance is greater because there is less fluid pressure at the stern.

A recent paper [13] provides physical insight into the cause of the time oscillation of the wave resistance. Towing tank experiments mentioned in [13] showed that whenever a ship (moving at constant speed) had an abrupt start or passed over an irregularity in the channel bottom, forces acting on the struts holding the ship model showed a force response localized in time followed by a slowly decaying almost periodic response which was called "ringing." As mentioned in [13], "The circumstances under which ringing occurs give a hint as to the physical cause. An abrupt start, a so-called "hard start," piles up the water in front of the ship model. This water must then dissipate itself in some fashion. Similarly, when the model passes over an obstruction, the water between the obstruction and ship is squeezed upwards and again must dissipate itself." Ringing is primarily a towing tank phenomenon and results mainly from the interference of multiply reflected waves (from the channel sidewalls) with each other and with the primary wave (resulting from the disturbance at the bow). Ringing occurs for an abrupt start in water of any depth. The period of the ringing is a function of (1) constant speed of the ship model, (2) depth of channel, (3) length of ship model, and (4) width of channel. Based on results presented in [13] the nondimensional period of ringing appears to be (for the Fr range of the present paper) on the order of several ship lengths travelled (i.e., several units of nondimensional time) and increases with increasing Froude number. The channel width of 1.6 ship lengths, as used in this paper, is not wide enough to

$\Delta t = 0.015$ during one complete fluctuation. The wave resistance is smallest at

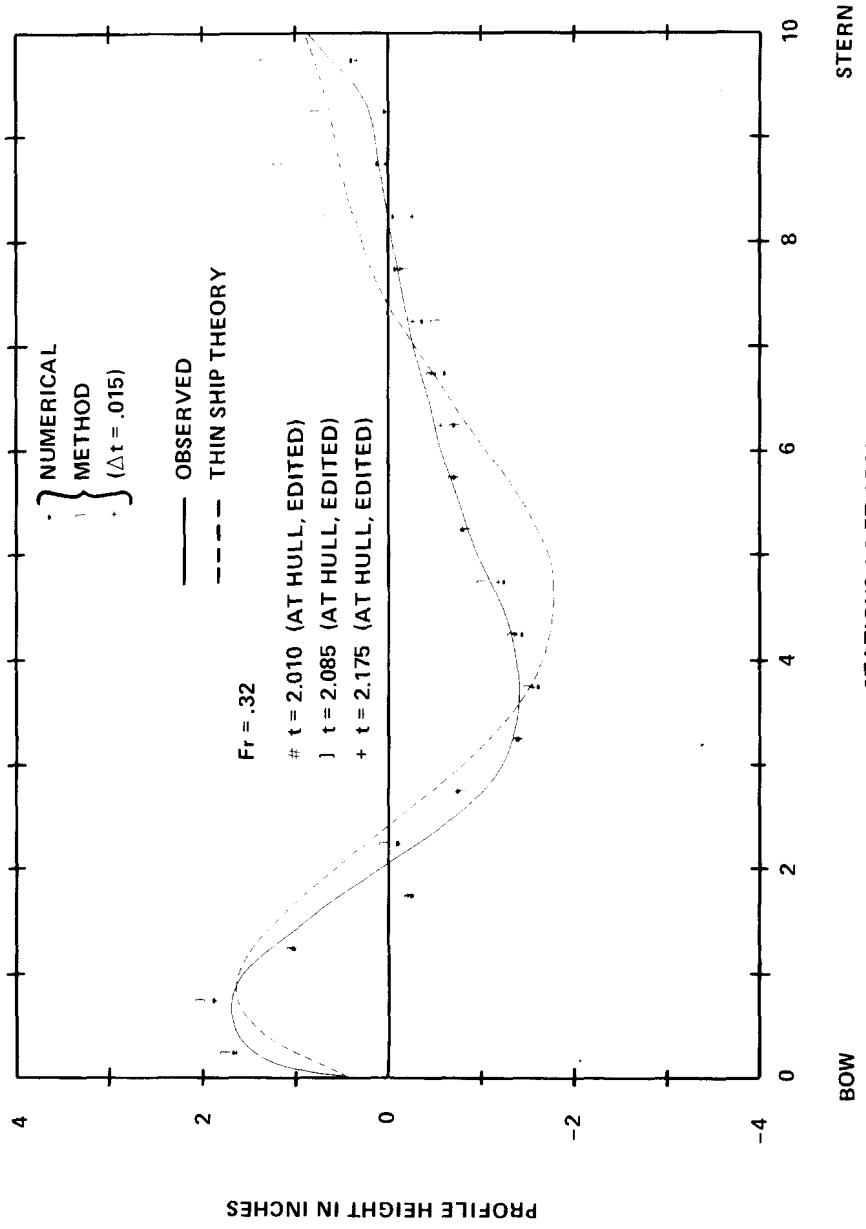

FIG. 8. Oscillation of stern wave profile at the hull causing fluctuation in C_R curve for $\mathrm{Fr} = 0.32$.

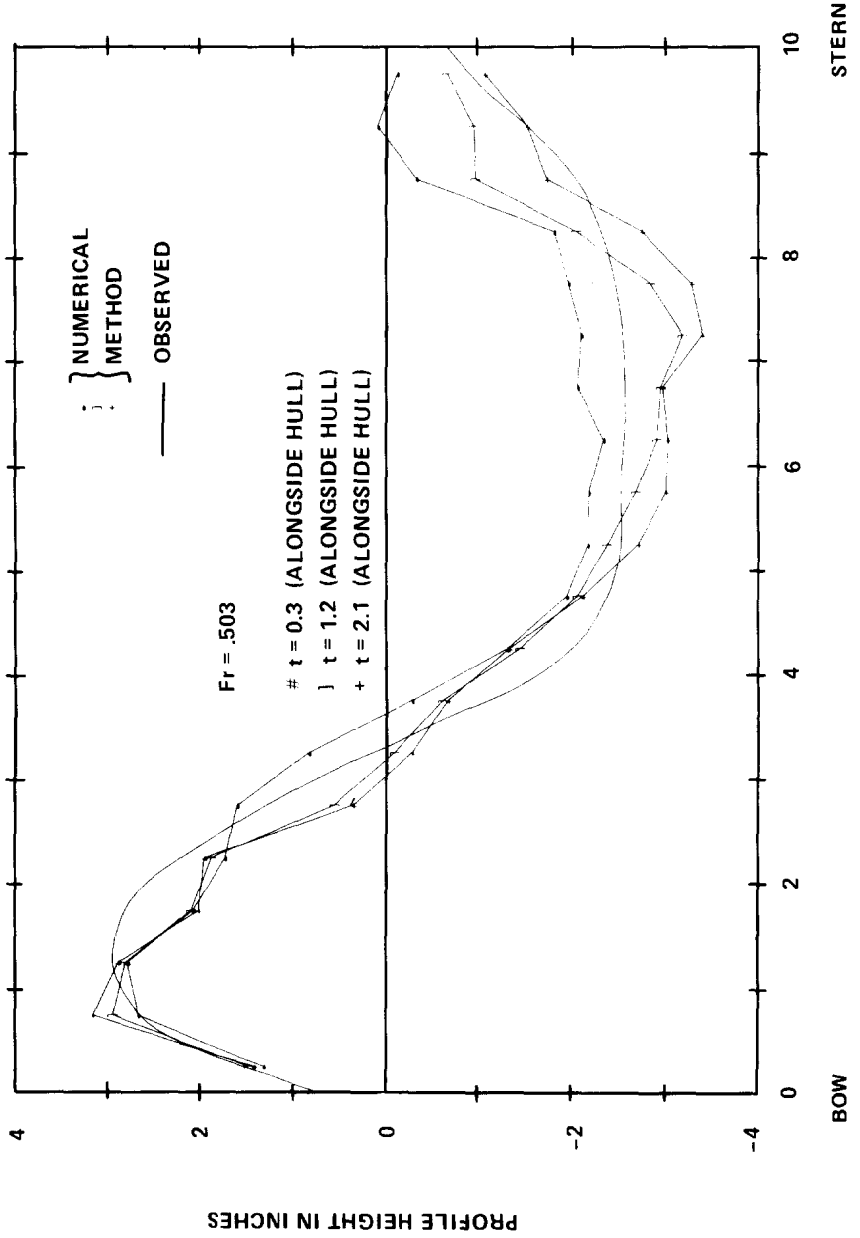

FIG. 9. Time sequence of wave profiles alongside the hull for Fr = 0.503.

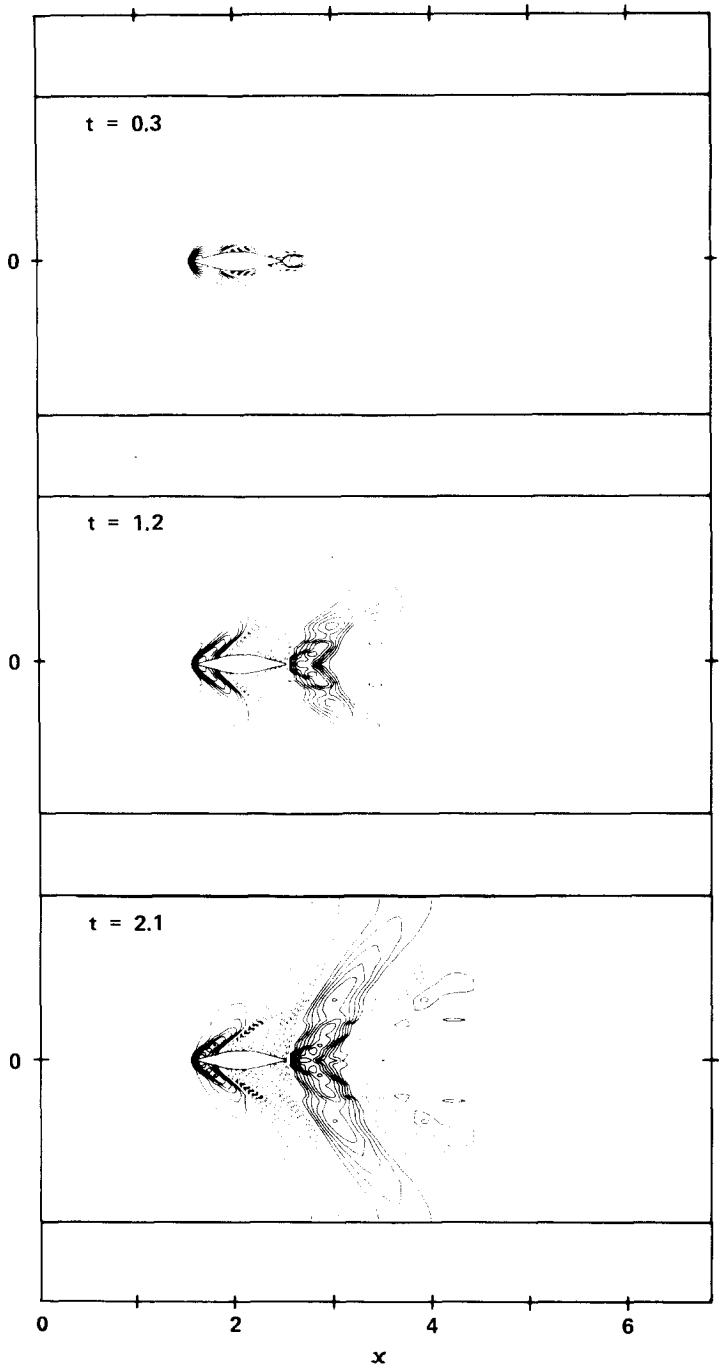

FIG. 10. Time sequence of free surface contours for Fr = 0.503.

$t = 2.085$ (when the stern wave is highest) and greatest at $t = 2.010$ and 2.175 (when the stern wave is lowest). The stern wave is fluctuating much more rapidly than Wehausen's [12] thin ship analysis theory predicts. The fluctuations are independent of the time step. The period of the fluctuations in the wave resistance curves of Fig. 7 are nearly independent of Froude number and are quite short (<0.2 the time to travel

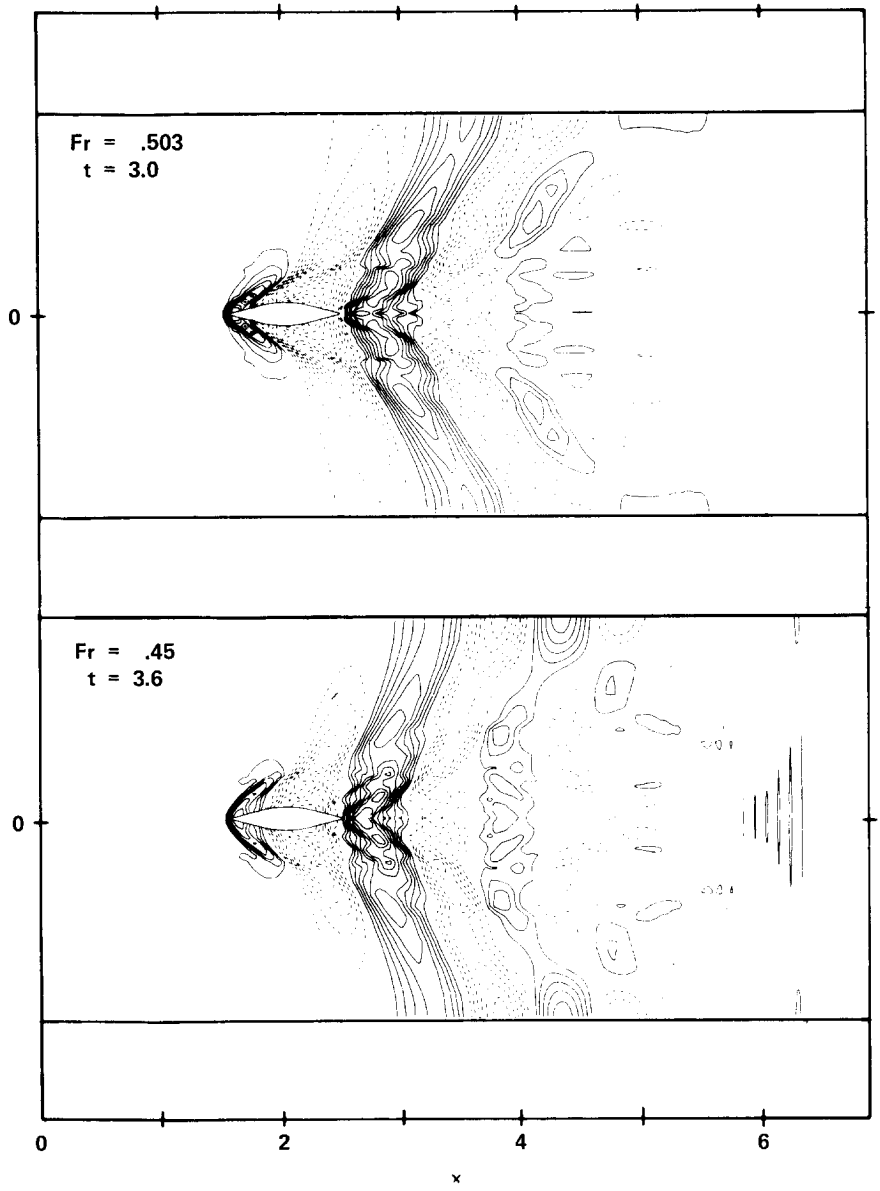

FIG. 11. Late time free surface contours for Fr = 0.503 at $t = 3.0$ and Fr = 0.45 at $t = 3.6$.

a ship length). Therefore the fluctuations don't appear to be explainable by either the ringing phenomenon or Wehausen's asymptotic expansion.

Figure 9 shows an early time sequence of wave profiles alongside the hull for $Fr = 0.503$; Fig. 10 shows nondimensional surface wave elevation contour plots for the same time sequence and Froude number. Figures 11 and 12 show late time

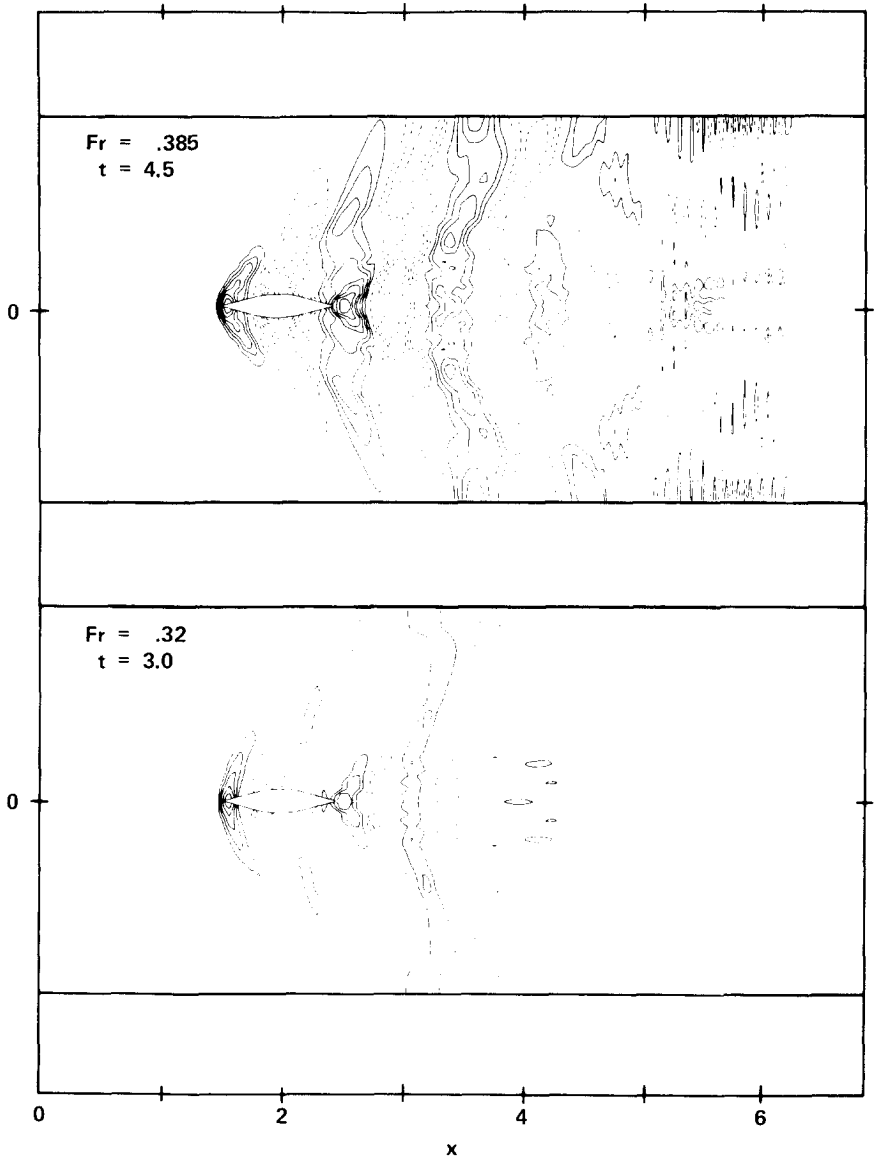

FIG. 12. Late time free surface contours for $Fr = 0.385$ at $t = 4.5$ and $Fr = 0.32$ at $t = 3.0$.

nondimensional surface wave elevation contour plots for the four Froude numbers. In Figs. 10–12 the entire channel is viewed aerially and channel sidewalls are shown. The channel width is 1.6 ship lengths, and, for viewing convenience, is portrayed in the figures as almost twice as large as it should be. The solution is computed in only one-half of the channel due to the symmetry conditions. Countour levels plotted (lines of constant surface elevation) had values of $0.002K$ with $K = \pm 1, \pm 2, \ldots$. Solid lines represent positive contour levels indicating wave crests and dotted lines represent negative contour levels indicating wave troughs.

Divergent and transverse wave systems are present in all the contour plots of Figs. 10–12. The transverse waves are those waves which are essentially two-dimensional and have wave crests and troughs approximately perpendicular to the center plane ($z = 0$) of the channel. These waves progress downstream from the ship at approximately half the speed of the ship in all the contour plots of Figs. 10–12 which is in agreement with the theory for two-dimensional harmonic progressive waves [6]. (The ship moves its length each unit of time.) The measurement of the downstream advancing wave front is made along the channel center plane ($z = 0$), lowest level isolated contours of either sign far downstream being ignored. The divergent waves are due to the three-dimensionality of the problem. For $\mathrm{Fr} = 0.385$ and $t = 4.5$ and $\mathrm{Fr} = 0.45$ at $t = 3.6$ in Figs. 12 and 11, respectively, lowest level reflections off the downstream boundary can be seen at $x = 6.4$ far from the ship due to the use of Eq. (15). To obtain very long time histories it might be necessary to apply a wave damping technique at the downstream boundary.

Figures 13–16 show perspective plots of the water surface for the four Froude number cases at the latest times computed. The viewer's eye position for Figs. 13–16 is at the point $(x, y, z) = (4.3, 0.3, 0.63)$ (i.e., the eye position is 4.3 ship lengths downstream in the x-direction from $x = 0$, 0.3 ship lengths above the plane $y = 0$, and 0.63 ship lengths from the center plane $z = 0$. The center of the ship is located 2.025 ship lengths downstream in the x-direction from $x = 0$.) The ship is shown as a cylindrical projection of the ship hull outline at $y = 0$ (i.e., Eq. (23) with $y = 0$). The mean level $y = 0$ at the ship is located five grid intervals Δy down from the top of the cyclindrical projection shown. Actual grid intervals $\Delta x = 0.05$ and $\Delta y = 0.005$ are shown along the sides of the ship. The bow and stern ends of the ship are shown slightly open, because the bow and stern edges do not contain grid points. The perspective and contour plots were made by using the Interactive Data Display System (IDDS) developed by Mr. Melvin Haas, Ms. Mary Beth Marquardt, and Mr. Richard VanEseltine at the David W. Taylor Naval Ship Research and Development Center in Bethesda, Maryland.

All computations were performed on the Texas Instruments Advanced Scientific Computer (TI-ASC) at the Naval Research Laboratory in Washington, D.C. This computer has a parallel processor option which increases computing power significantly. This option was not used here due to the lack of a Fast Fourier Transform package to take advantage of the parallel processor. Without this option the TI-ASC has a computing speed roughly 25 % faster than that of the IBM 360-91. The following amounts of computer time were required to advance the solution from

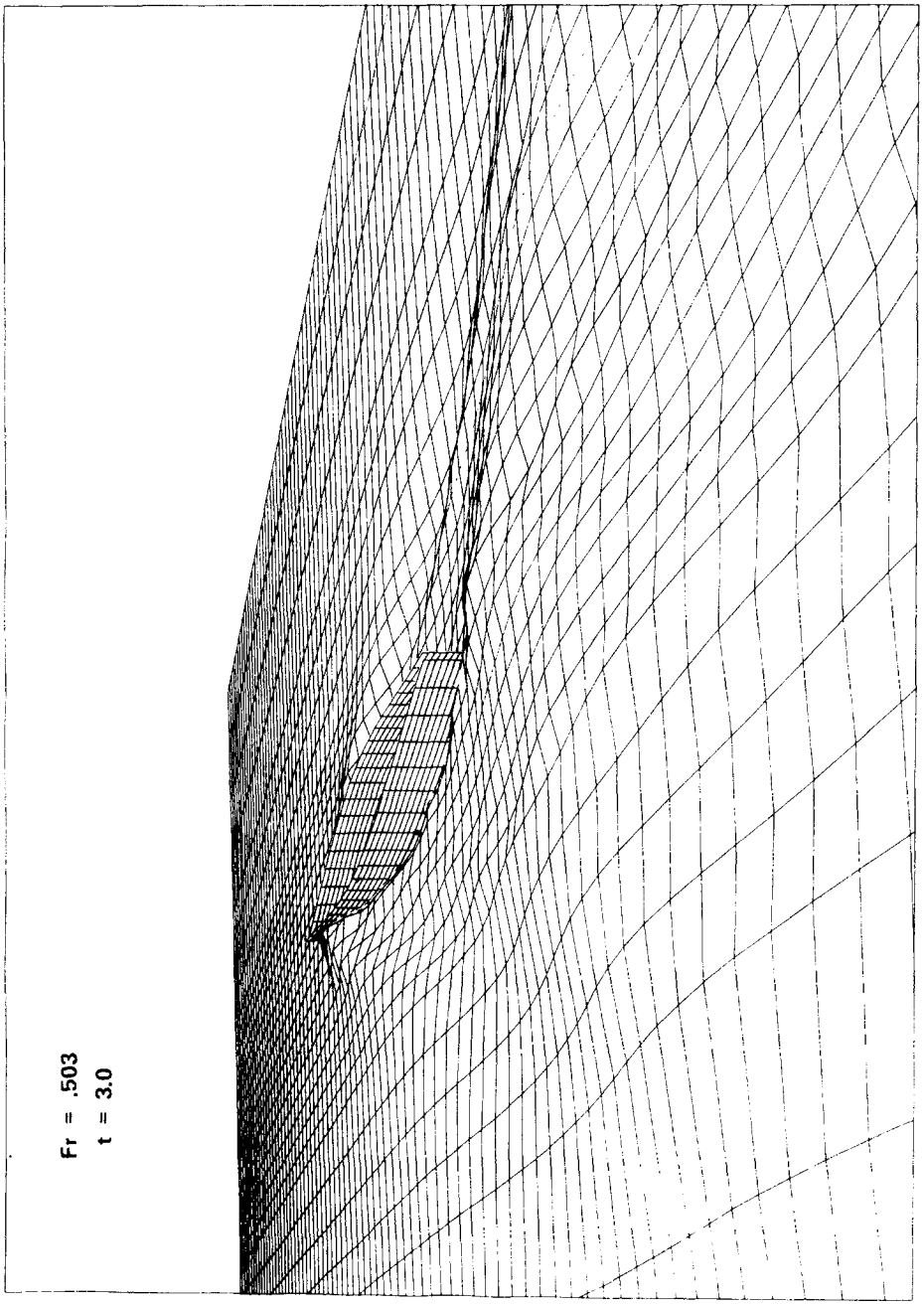

FIG. 13. Perspective plot of free surface for $\mathrm{Fr} = 0.503$ at $t = 3.0$.

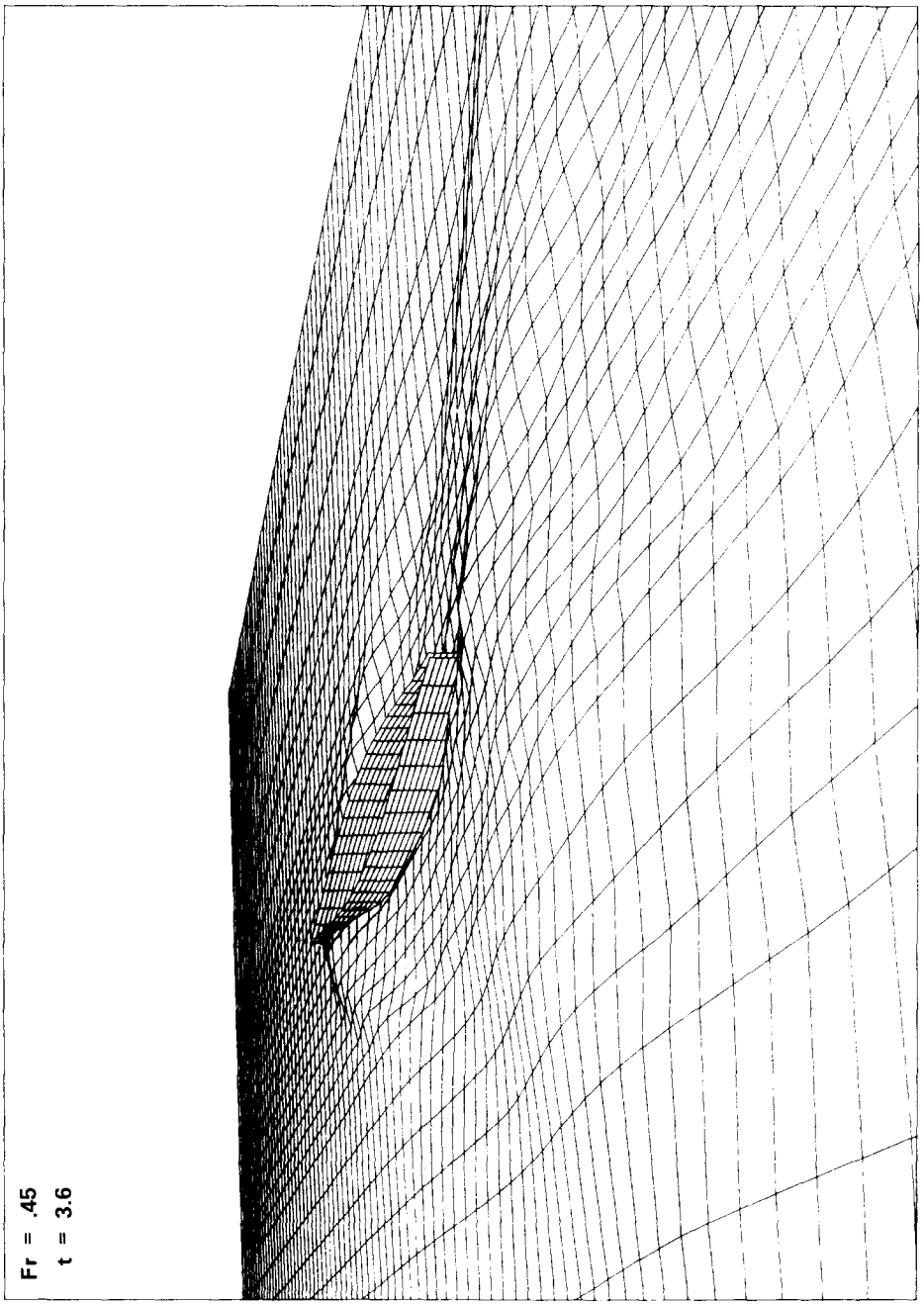

FIG. 14. Perspective plot of free surface for Fr = 0.45 at $t = 3.6$.

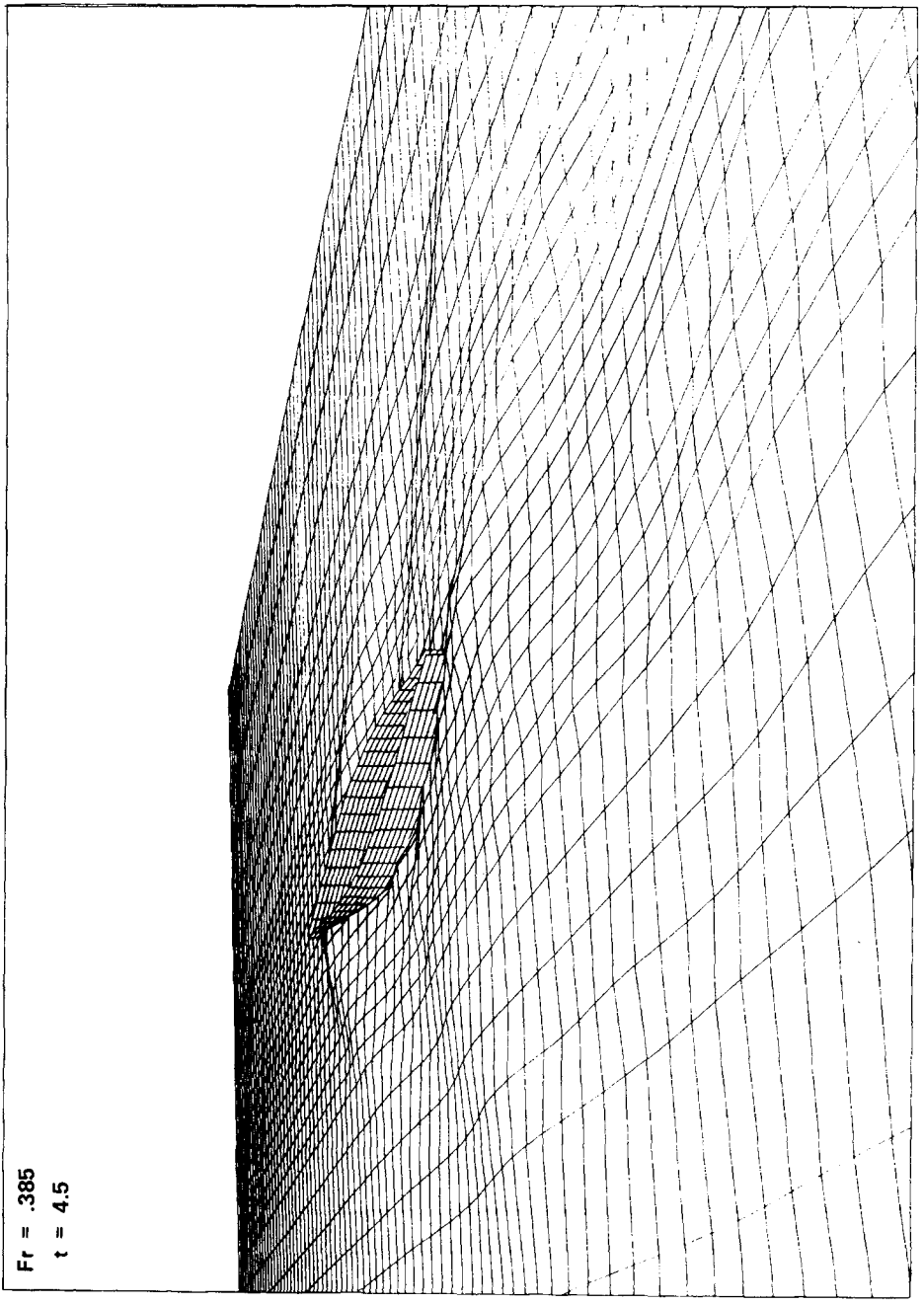

FIG. 15. Perspective plot of free surface for $\mathrm{Fr} = 0.385$ at $t = 4.5$.

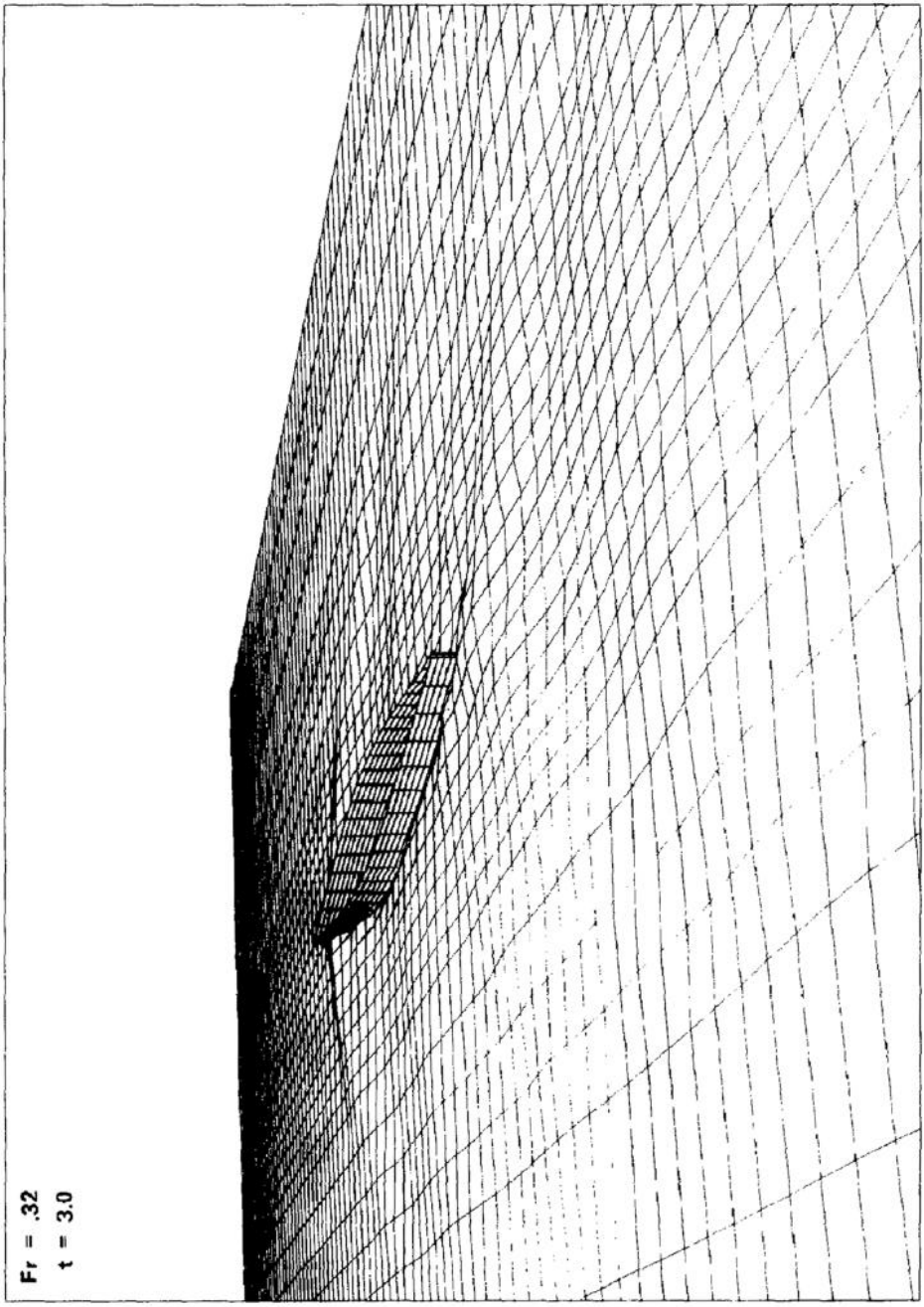

FIG. 16. Perspective plot of free surface for $\mathrm{Fr} = 0.32$ at $t = 3.0$.

$t = 0.0$ (using $\Delta t = 0.03$) to the final recorded values of t for the four Froude number cases:

Froude number	Number of time steps	Computer time
0.503	100 ($t = 3.0$)	12 min, 41 sec
0.45	120 ($t = 3.6$)	16 min, 12 sec
0.385	150 ($t = 4.5$)	24 min, 33 sec
0.32	100 ($t = 3.0$)	19 min, 59 sec

The higher Froude numbers require less computer time because they use fewer computational cycles per time step. In addition, a one-time computer preprocessing step, which used 3 min, 19 sec of computer time, was required to compute C_S and its inverse C_S^{-1} and eigenvectors and eigenvalues, etc. for use in the imbedding technique. A one-time computation for the double model velocity problem required 3 min, 33 sec.

5. Conclusions

The use of the imbedding technique for satisfying the ship hull condition, in combination with the double model velocity linearization of the free surface equations, has been shown to be effective in computing three-dimensional ship wave generation. This finite difference scheme is efficient with respect to both computer time and storage used. The scheme, with minor modifications, can calculate free surface flow past an accelerating ship in addition to an abruptly started ship considered here. Approximately steady states have been obtained at the ship hull at the higher Froude numbers, and wave resistance has been computed. Results obtained with the double model linearization are generally more accurate than those obtained with the use of a free stream linearization for the free surface as in [5].

Acknowledgments

The author would like to thank Messrs. Melvin Haas and Richard VanEseltine and Ms. Mary Beth Marquardt for the use of their plotting programs. The author also would like to thank Ms. Anne Laney for her careful typing of the manuscript. This work was supported by the Numerical Naval Hydrodynamics Program at the David W. Taylor Naval Ship Research and Development Center. The program is sponsored jointly by DTNSRDC and the Office of Naval Research.

References

1. K. J. Bai and J. H. McCarthy (Eds.), "Proceedings, Workshop on Ship Wave Resistance Computations, David W. Taylor Naval Ship Research and Development Center, Bethesda, Md., Nov. 13–14, 1979."

2. J. V. WEHAUSEN AND N. SALVESEN (Eds.), "Proceedings, Second International Conference on Numerical Ship Hydrodynamics, University of California, Berkeley, Calif., Sept. 19–21, 1977."
3. J. K. LUNDE, "The Linearized Theory of Wave Resistance and Its Application to Ship-Shaped Bodies in Motion on the Surface of a Deep, Previously Undisturbed Fluid," Technical and Research Bulletin No. 1–18, SNAME, 1957.
4. S. OHRING AND J. TELSTE, *Comput. Methods in Appl. Mech. Eng.* **21** (1980), 315.
5. S. OHRING AND J. TELSTE, *in* "Proceedings, Second International Conference on Numerical Ship Hydrodynamics, University of California, Berkeley, Calif., Sept. 19–21, 1977" (J. V. Wehausen and N. Salvesen, Eds.), pp. 88–103.
6. J. J. STOKER, "Water Waves," Interscience, New York, 1957.
7. B. L. BUZBEE *et al.*, *SIAM J. Numer. Anal.* **8** (1971), 722.
8. D. P. O'LEARY AND O. WIDLUND, *Math. Comput.* **33** (1979), 849.
9. J. R. SHEARER, *North-East Coast Inst. Eng. Shipbldg., Trans.* **67** (1951), 43.
10. C. VON KERCZEK AND E. O. TUCK, *J. Ship Res.* **13** (1969), 284.
11. R. TIMMAN, "Water Waves," Department of Mathematics Lecture Notes, University of Delaware, Newark, Del., 1971.
12. J. V. WEHAUSEN, *J. Ship Res.* 7 (1964), 38.
13. O. J. SIBUL, W. C. WEBSTER, AND J. V. WEHAUSEN, *Schiffstechnik* **26** (1979), 179.